Evaluating the Mechanistic Whole-Brain Model of Empirical MEG Data

Weronika Kowalczuk,[1] Tobias Meeks,[1] and Shayan Shafquat[1]

[1]*School of Mathematical Sciences, University of Nottingham, Nottingham, NG7 2RD, UK*

(Dated: March 9, 2024)

This report delved into the realm of resting-state brain activity and its underlying brain dynamics, specifically aiming to reproduce the groundbreaking work of Deco [1]. Their paper introduced two computational models aimed at providing a theoretical framework for studying brain oscillations, functional connectivity and synchrony. One model was focused on a single-frequency notion, wherein brain oscillations are assumed to occur only at one specific frequency. The second model, however, incorporated the knowledge that brain oscillations can occur at varying frequencies for different nodes. It is this latter multiple-frequency model that they found was most similar to their collected magnetoencephalography (MEG) data. This report's employed methodology encompassed both Python and MATLAB (for higher reproducibility purposes) and not only reproduced but went beyond the analysis of the original Deco [1] paper. Through the exploration of bifurcation diagrams, nullclines and parameter variations (paying particular attention to noise) we were able to obtain findings indicative of a more successful multiple-frequency model, whilst uncovering crucial oversights in the original paper [1]. Our findings show that while the computational model could be replicated to exhibit behaviour similar to empirical evidence and Deco's [1] own computations, significant challenges were encountered in achieving such results, and a comprehensive analysis revealed the model's overall low replicability. In light of these challenges, we question whether the Wilson-Cowan model may offer a more reliable alternative. The implications of our findings extend to the broader understanding of resting-state brain dynamics. By shedding light on the limitations and challenges in replicating computational models, our study emphasises the importance of transparent reporting and sharing of supplementary code in scientific research, so we can advance our understanding of resting-state brain activity.

I. INTRODUCTION

A key area within practical biomedical modelling is the focus on simulating activity in the most intricate organ in the human body: the brain. Research frequently delves into the complexities of ongoing brain activity during a range of tasks, as well as our state of quiescence, often referred to as the "resting state". In 2017, Deco [1] and their team conducted research into the fundamental mechanisms underlying envelope correlations in on-going brain activity during such resting-state. They collected their own empirical evidence via magnetoencephalography (MEG) in an attempt to recreate this collected data computationally through the use of simplified mathematical formulae. Such research is vital to conduct at this prime time, as our scientific applications begins to shift towards an artificial intelligence era [2]. When it comes to detailed computational modelling, research thus far focused on the intricacy of network topologies and their connections, with many studies successfully replicating electrophysiological measurements through the use of mathematical simplification [3, 4]. The frequency of these observed oscillations relies on time constants, such as the feedback delay. This describes the excitatory-inhibitory loops within neural networks, wherein excitatory signals stimulate the firing of neurons, whilst inhibitory signals suppress this neuronal activity, consequently meaning that the difference in effects for the subsequent neuronal activity can introduce delays within our system's response. It is therefore crucial to understand these inner dynamics of, say feedback loops and their delays, to elucidate how our neural circuits process information and regulate our behaviour [1].

It is this notion that inspired Deco's [1] research, as they attempted to investigate locally generated oscillation interactions at a macroscopic level – hence their "whole-brain mechanistic model". The way this is generally approached is through the use of differential equations that are able to represent neuronal population relationships, thus simplifying the complexity of spiking neuron models and using a "neural-mass model" [5, 6, 7, 1]. A key ingredient when building such models is a structural brain network characterized by long-range brain connections with embedded conduction delay, within which neural populations are placed at each network node, and assumed to spontaneously oscillate [6] - this of course bares immediate consequences of model validity, as the intricacy of neurons becomes simplified, and assumptions are made. Hence why many studies compare these models to empirical evidence [6, 1]. However, we cannot simply rely on single studies to computationally simulate an organ that scientists have been trying to recreate for years. This abundance of research has the necessity to be continually reviewed and replicated.

Studies prior to Deco [1] have also investigated the electrophysiological basis of resting state networks with the use of MEG. Brookes [8] demonstrated a significant correlation between amplitude envelope of neural oscillatory signals across brain regions which were spatially separated, concluding a neural oscillatory basis for functional connectivity in resting state networks. They also

revealed the vital role that synchronised electrical activity plays in coordinating brain regions within specific networks. Other studies have emphasised the neural and physiological factors underlying resting state brain activity, specifically pointing to neural dynamics at each individual node, looking at the structural connectivity of the brain's anatomical network, influence of physiological noise on resting state activity and considerations of slow fluctuations (<0.1Hz) in physiological signals [7]. Moreover, frequency bands have been a key parameter varied within studies, as it has been identified that there is a complex interplay of information exchange across different frequency bands and brain regions [1, 9].

In considering the practical implications of Deco's [1] model, it is essential to recognise the need for further investigation and validation, given the limitations and still unanswered questions arising from their study, and often inherent in biomedical modelling research. The most notable, and potentially most significant limitation lies in the simplification of intricate neuronal populations to achieve the computational model itself. By assuming certain dynamics and connectivity patterns within brain networks, computational models may fail in capturing the entire complexity of real-world scenarios, potentially leading to disparities between simulated and observed data. Whilst Deco [1] as well as other scientists [8] have compared their model outputs to empirical MEG data, their reliance on a single dataset for model validation poses a constraint on the generalisability of their findings. This risk emphasises the necessity for replicating their results, to provide further supporting evidence for their multi-frequency mechanistic model, which challenges thus far single-frequency approaches [10]. Moreover, their paper struggles to address the sensitivity of their model outcomes to parameter choices, such as noise or global coupling parameters, which raises concerns about the reproducibility of their findings.

Addressing these limitations through exploring wider parameter ranges, as well as confirming basic system behaviour using Hopf bifurcations, nullclines etc., could offer insights into the robustness of the model and confirm the optimal settings they observed. Overall, this can refine our knowledge of biomedical modelling by evaluating their proposal against our own findings, which would thus advance the applicability of the study's results to broader contexts in neuroscience and brain research. The following paper therefore aims to reproduce the findings of Deco [1] using various coding languages (specifically Python and Matlab) and comparing them against other computational model outcomes that aim to imitate resting-state brain activity similar to that of MEG scans. The model and methodological approach will covered in the next section, including the assumptions which had to be made along the way, followed by the results obtained and a general discussion of how this compares to the original Deco [1] paper, their empirical MEG evidence and the Wilson-Cowan model [11]. Suggestions for future research will also be made.

II. METHODOLOGY

A. The Model

The dynamics of nodes of the brain have been modelled in a way to exhibit a supercritical Hopf bifurcation, wherein beyond a specific parametric point, a stable steady state destabilises and periodic stability is established. In other words, the complex eigenvalues of the steady state transition from having a negative real part to a positive real part. Therefore, with a noise-induced model, one should see a transition from generally noisy behaviour to oscillatory behaviour. To model said brain nodes, we make use of the Stuart-Landau model:

$$\frac{dz_j}{dt} = z(a_j + i\omega_j - |z_j^2|) + \beta\eta_j \tag{1}$$

where,

$$z_j = \rho_j e^{i\theta_j} = x_j + iy_j \tag{2}$$

Through the expansion of z_j into the cartesian coordinate system, we get a system of ODEs:

$$\frac{dx_j}{dt} = (a_j - x_j^2 - y_j^2)x_j - \omega_j y_j + G\sum C_{ij}(x_i - x_j) \tag{3}$$

$$\frac{dy_j}{dt} = (a_j - x_j^2 - y_j^2)y_j + \omega_j x_j + G\sum C_{ij}(y_i - y_j) \tag{4}$$

Values x_j represent the MEG signal of node j. a_j is the parameter used to initiate the bifurcation: for $a_j < 0$ the system reaches a stable steady state at $(x_j, y_j) = (0, 0)$, and at $a_j \geq 0$ the system showcases oscillatory behaviour, reaching an unstable steady state with stable periodicity. A fixed value of $a = 0$ is used within the simulations, given that it represents the system at the bifurcation point where the system transitions into an oscillatory state. C_{ij} is the structural matrix, where entry ij represents the fibre density between regions i and j. G is the coupling strength of the structural matrix, and a fixed value of $G = 0.5$ has been used throughout the report. $\omega_j = f_f 2\pi$, where f_f is the initial carrier frequency of the node.

After plotting the nullclines and x over time (Figures 3 and 4), we observe analogous behaviour of the system with that of the Hopf bifurcation (Figure 2), thus verifying that the computational modelling of the system has been executed correctly, and patterns of behaviour can be identified. As can be seen in Figure 3, when α reaches a value of 0 or above, trajectories show a sustained oscillatory pattern – displaying a limit cycle periodic in nature. When α reaches negative values (e.g., -1 as in Figure 3) we see trajectories increasingly quickly tend

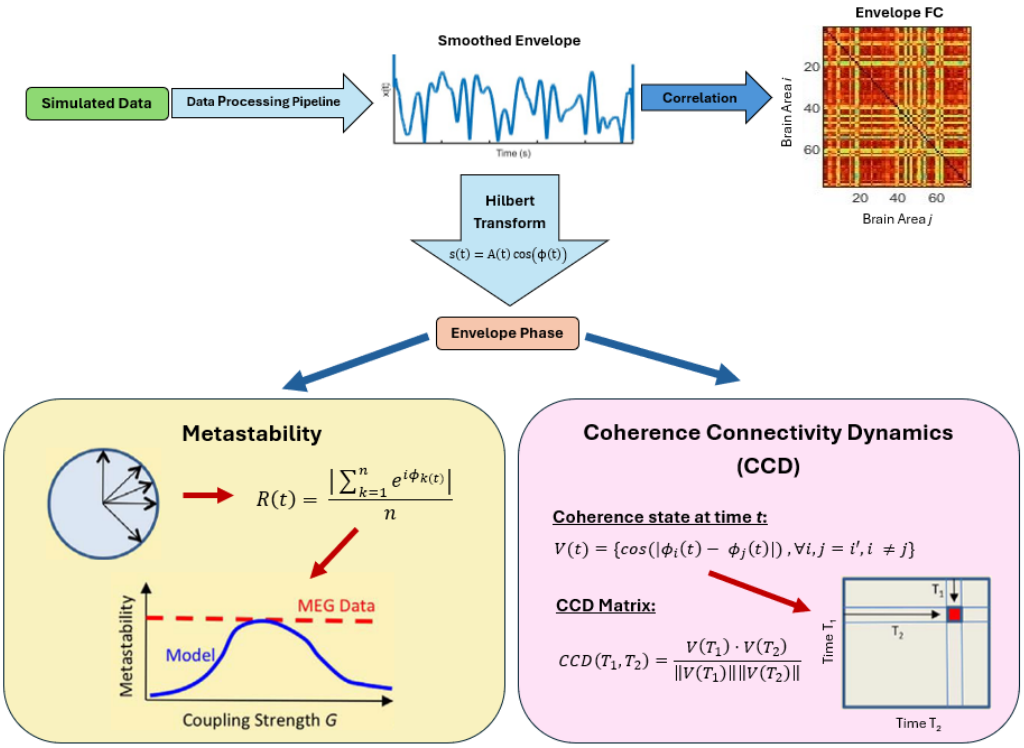

FIG. 1: **Data Analysis Pipeline.** After solving the system of ODEs using the Euler-Maruyama method, the oscillatory solution is band-passed between a specified range. The amplitude envelope of the band-passed oscillation is low-passed at 0.2Hz. The envelope FC is the Pearson's correlation between the low-passed amplitude envelope of each brain region. The instantaneous envelope phase $\phi_k(t)$, the angle of the Hilbert-transformed slow envelope, is then calculated, and is used in the calculation of metastability, the standard deviation of the Kuramoto parameter R(t) showing global synchronisation; and the coherence connectivity dynamics (CCD), a correlation between the coherence of the signals from each brain region. Modification of figure in [1].

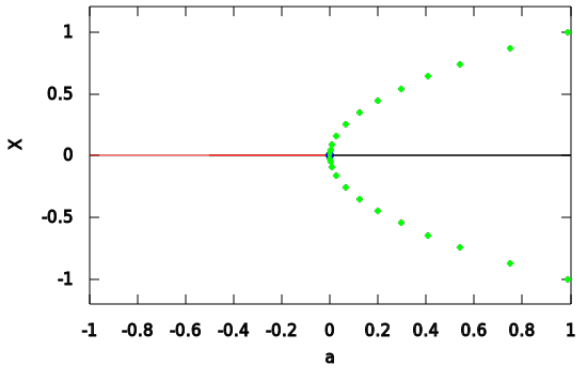

FIG. 2: **A Supercritical Hopf bifurcation plot for Stuart-Landau model.** The system dynamics at the critical juncture of a = 0, where a is the bifurcation parameter. Here, the system transitions from a stable equilibrium to a periodic regime, as evidenced by the emergence of a limit cycle. This marks the point at which the system's behaviour shifts from a static state to oscillatory motion.

towards a stable, steady state. This significant impact of the α parameter is also supported in Figure 4.

Wilson and Cowan is an activity-based framework used to model the dynamics of the brain nodes. It differentiates between the excitatory and inhibitory neuron populations while also considering their refractory periods [11]. To mathematically describe this model, we use the following set of ordinary differential equations (ODEs):

$$\tau_E \frac{dE_i}{dt} = -E_i + f_E(W_{EE}E_i - W_{EI}I_i + P_E + G\sum_j C_{ij}E_j) \tag{5}$$

$$\tau_I \frac{dI_i}{dt} = -I_i + f_I(W_{IE}E_i - W_{II}I_i + P_I) \tag{6}$$

The equations define $E(t)$ 5, a time-dependent variable that signifies the proportion of excitatory neurons firing at any given moment, and $I(t)$ 6, which analogously represents the firing proportion of inhibitory neurons. These constants, C_{ab}, represent the synaptic strength from neurons in population b to those in population a, with a, b either being E or I. The functions f_a

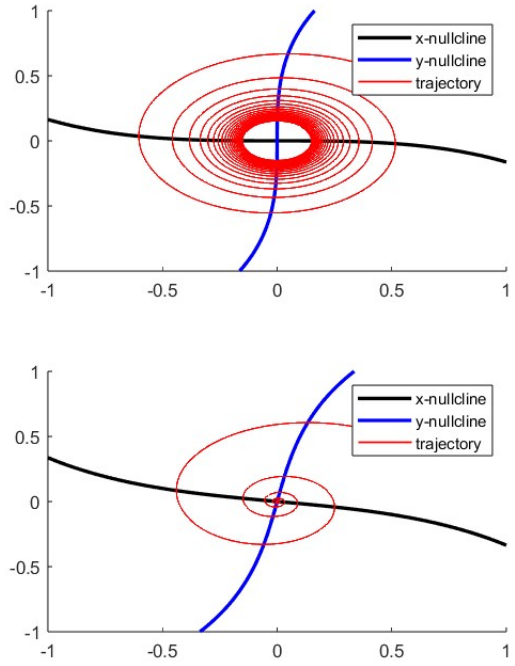

FIG. 3: **Nullcline subplots.** The nullclines of the Stuart-Landau system of ODEs. (Above) Trajectories showing the unstable steady state found when $a_j = 0$. (Below) Trajectories showing the unstable steady state found when $a_j = -1$. The steady state is at $(x_j, y_j) = (0, 0)$ and visualises the supercritical hopf bifurcation.

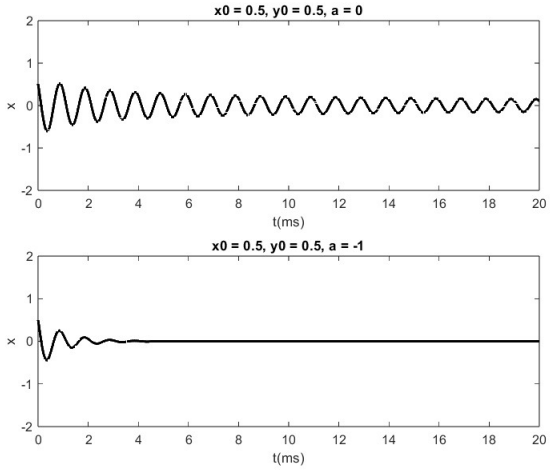

FIG. 4: **ODE solutions to Stuart-Landau model without noise.** (Top) ODE solutions when $a = 0$. A sustained oscillation is observed. (Bottom) ODE solutions when $a = -1$, a gradual approach to the steady state $(x_j, y_j) = (0, 0)$.

denote the fraction of neurons in population a receiving at least a threshold excitation level at any moment, typically modelled as a nonlinear function (sigmoid). In these equations, τ_E and τ_I are the time constants for the excitatory and inhibitory neurons, respectively, and P_a reflects external inputs that might be variable over time.

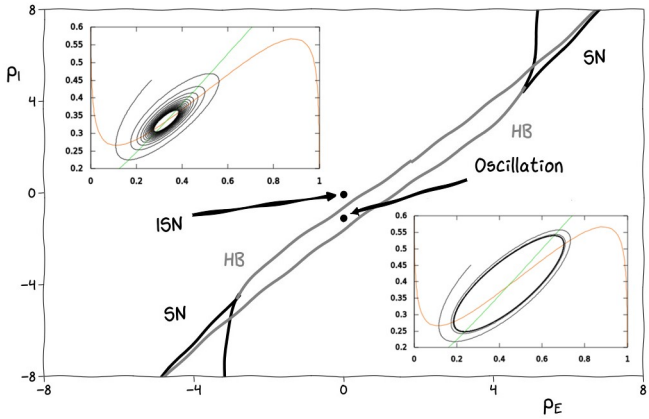

FIG. 5: **A supercritical Hopf bifurcation plot for the Wilson-Cowan model [11].** The system dynamics depend on the bifurcation parameters p_e and p_i with the presence of Hopf bifurcation and Saddle nodes. The insets depict the phase plane (E-nullcline in red and I-nullcline in green) for a parameter set supporting an ISN with (pE , pI) = (0, -0.647) and a parameter set supporting a sustained oscillation with (pE , pI) = (0, -1). Black lines denote numerically determined trajectories. Modified image from [11].

B. Euler Maruyama method

The Euler-Maruyama (EM) method [12] modifies the classic Euler algorithm for ordinary differential equations to accommodate stochastic differential equations, which are influenced by random perturbations. This method captures the randomness through a noise term, typically represented by a Wiener process. The Wiener process is described by a normal distribution with a mean of zero and a time-dependent variance, reflecting the system's stochastic nature.

The Euler-Maruyama method is appreciated for its computational simplicity and straightforward implementation. It differentiates from the deterministic Euler method by including a stochastic term to account for the random fluctuations in the system dynamics.

For a general stochastic differential equation:

$$dx_t = a(x_t, t)dt + b(x_t, t)dW_t, \tag{7}$$

where x_t is the state variable at time t, $a(x_t, t)$ represents the drift coefficient, $b(x_t, t)$ signifies the diffusion coefficient, and dW_t is the incremental effect of the

Wiener process, the Euler-Maruyama approximation is expressed as:

$$x_{t+\Delta t} = x_t + a(x_t, t)\Delta t + b(x_t, t)\sqrt{\Delta t}\,\xi_t, \qquad (8)$$

with ξ_t being a random draw from a standard normal distribution. The term $\sqrt{\Delta t}$ ensures that the noise term's variance scales with the timestep, in alignment with the properties of the Wiener process.

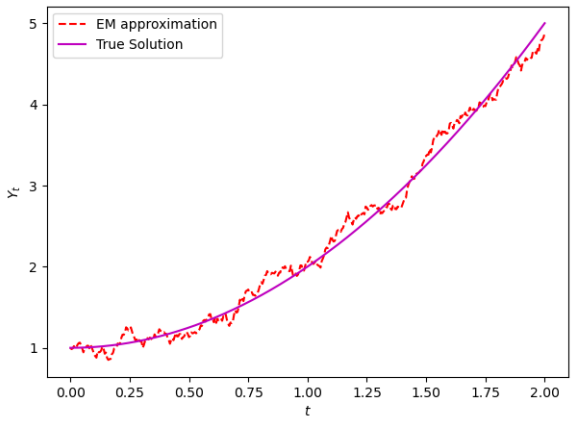

FIG. 6: **Comparison of the Euler-Maruyama Approximation with the Analytical Solution.** It compares the true solution of the stochastic differential equation with its Euler-Maruyama (EM) approximation over time. The EM method closely follows the exact trajectory, demonstrating its effectiveness in approximating solutions with noise components.

By employing this methodology, we incrementally simulate the evolution of a system's state, integrating both its deterministic trajectory and stochastic variations.

C. Data Processing

Band-pass filtering allows us to focus on specific ranges of frequencies, amplifying signals within said range and allowing more detailed analysis within that range. Throughout the results section of the report, ranges of $[f_{fundamental} - 2Hz, f_{fundamental} + 2Hz]$ have been used, with $f_{fundamental} = 4 : 4 : 28$. Additionally, the amplitude envelope of the band-pass-filtered oscillation at each node is calculated using a Hilbert transformation, $s(t) = A(t)cos(\phi(t))$, where A(t) is the amplitude envelope, and $\phi(t)$ is the instantaneous phase. In some instances, the amplitude envelope is low-pass filtered at 0.2Hz as to only include slow fluctuations of the envelope. The low-passed oscillations are used in the calculation of the envelope functional connectivity of the nodes, since it has been shown to maximise resting-state functional connectivity [8].

D. Envelope Functional Connectivity

The envelope functional connectivity between each node was calculated as the Pearson's correlations of the low-pass-filtered amplitude envelopes of each node. The result is a correlation matrix, where the entry ij represents the functional connectivity between region i and j. A larger correlation value would imply a higher correlation between the two regions.

E. Synchronicity and Metastability

Looking at phase activity across regions over time provides insight into variability in global connectivity. The Kuramoto order parameter:

$$R(t) = \frac{|\sum_{k=1}^{n} e^{i\phi_k(t)}|}{n} \qquad (9)$$

with $\phi_j(t)$ representing the instantaneous phase of the band-passed amplitude envelope, is used to visualise said synchronisation between regions. A larger value would imply a higher level of global synchronisation. Metastability can be defined as the standard deviation of the Kuramoto parameter.

F. Coherence Connectivity Dynamics

The coherence state at time t is given by:

$$V(t) = \{\cos(\phi_i(t) - \phi_j(t)) \,|\, \forall i, j = j, i, i \neq j\} \qquad (10)$$

The CCD matrix is defined as:

$$CCD(T_1, T_2) = \frac{V(T_1) \cdot V(T_2)}{\|V(T_1)\|\|V(T_2)\|} \qquad (11)$$

The coherence connectivity dynamics (CCD) compares the time-dependent instantaneous phases of the amplitude envelopes of the band-passed signals for each region. The CCD is calculated by the cosine similarity, at two given time steps, of the cosine of difference between instantaneous phases between all nodes. With a range between 0 to 1, a value close to 1 would imply a higher global connectivity between given time steps, and 0 the contrary.

III. RESULTS

A. Single Frequency Model

In the single-frequency model, a fixed value of 12Hz was used as the optimal fundamental frequency as decided in [1], meaning all brain regions are considered to be generating signals of the same frequency. The corresponding solutions of the dynamic system using the Euler-Maruyama method, with time step, $dt = 0.001$,

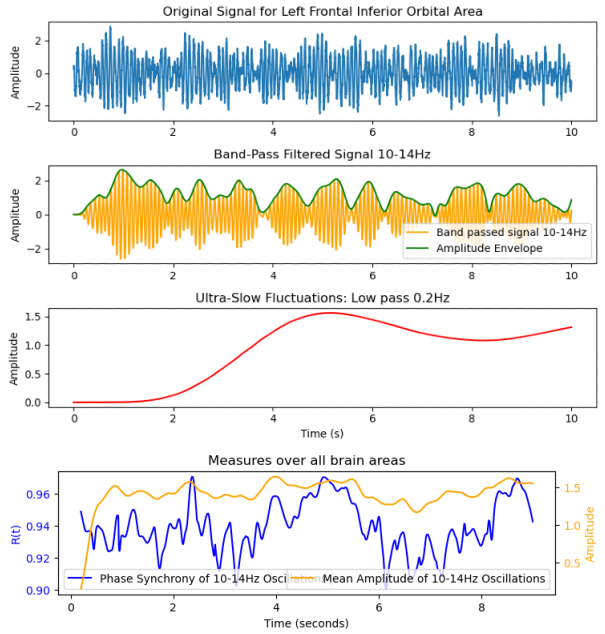

FIG. 7: **Simulated Signal in a brain area before and after band-pass and low pass filtering.** A blue trace illustrates a 10-second simulated signal from the Hopf model, tuned to a foundational frequency (f_f = 12 Hz) and a coupling constant (G) of 0.5. Post band-pass filtering within the 10-14 Hz range, the signal (depicted in yellow) and its amplitude envelope (shown in green) were derived via the Hilbert transform. These visualizations are specific to the Left Frontal Inferior Orbital Area. A further transformation, the low-pass filter set at 0.2 Hz, is applied to the amplitude envelope, yielding a smooth red curve. Additionally, the phase for the 10-14 Hz frequency range was calculated for each brain region through the Hilbert transform. The collective phase coherence was then quantified using the Kuramoto Order Parameter. Notably, a parallelism is observed between the synchrony metric (in blue) and the mean amplitude (in yellow) of the 10-14 Hz brain wave oscillations.

and sample rate $sample\_rate = 1/dt$, were band-passed within multiple narrowbands, and the envelopes for each band-passed oscillation were calculated. As can be seen in Figure 10, taking into account the mean correlation seen in Figure 15, band-passing the signals with narrowband $[10, 14]$ generates envelope functional connectivity more correlated between brain regions as well as to the structural connectivity data, especially for $\beta = 0.5$, validating the findings of Deco et al [1]. The effect of increasing the noise drastically can also be observed within the figure; not only does the correlation between the structural connectivity data and the envelope functional connectivity decrease, but general functional connectivity between regions depletes across band-passed ranges, indicating that the strength of the noise has overpowered the dynamic system. However, the mean correlations between the functional connectivity matrices and the structural connectivity data are generally low for all β and all band-passing ranges.

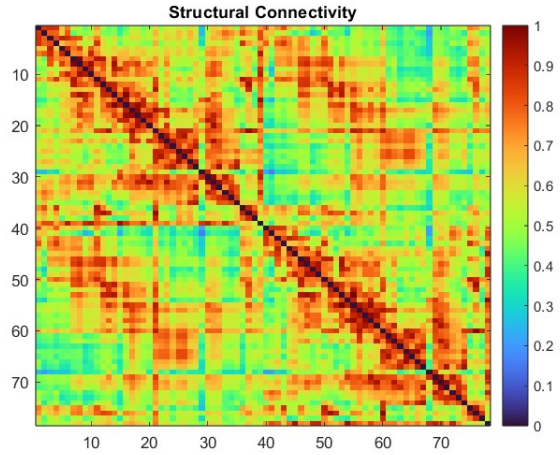

FIG. 8: **Structural Connectivity Heatmap.** The anatomical connectome data used in all the simulations was from the AAL atlas [13]

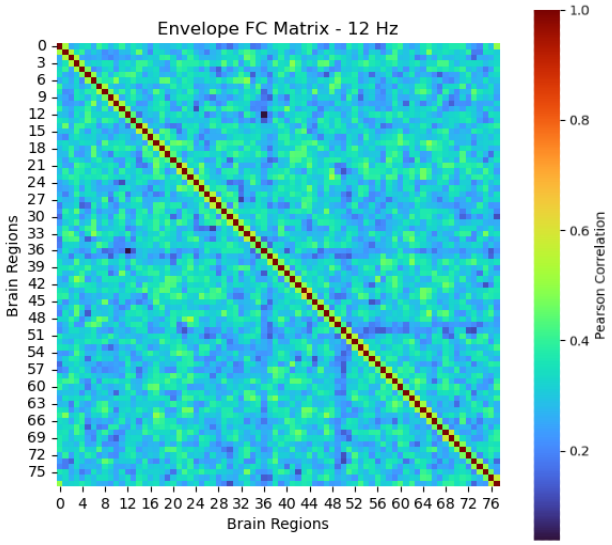

FIG. 9: **Functional connectivity Heatmap.** Simulations were run for f_f = 12 Hz, dt = 0.001, β = 3 and t_{max} = 300 secs. Zones of lesser correlation can be observed compared to the surrounding regions, and so a "cross" of lower correlations. This indicates that there are specific nodes that significantly lack functional connectivity with other nodes.

As for the CCD, Figure 11 shows the CCD matrix calculated on signals band-passed through the optimal range $[10, 14]$, simulated for 10 seconds. Expectedly, during close time steps, the signals are generally more synchronous than more distant time steps. This is es-

pecially notable at the beginning and end of the simulation. What is visible is a checkerboard pattern, representing the fluctuations in synchrony expressed between the regions of the brain; the regions of the brain become more or less synchronous periodically. If the simulation were run for a longer time period, the checkerboard pattern would become even more prevalent.

B. Multiple Frequency Model

The Multiple Frequency Model adapts to the simulation the knowledge that each brain region can generate multiple oscillations of different frequencies [1]. Within the model, each region is simulated at a set of different fundamental frequencies $f_{fundamental} = 4 : 4 : 28$. Then, the solutions to the system are band-passed at a more specified narrow-band of $[f_{fundamental} - 2, f_{fundamental} + 2]$ for each $f_{fundamental}$. The results of the envelope functional connectivity matrices can be seen in Figure 13. For $\beta = 0.5$, a sudden decrease in correlation before a general increase between brain regions can be seen with an increased $f_{fundamental}$, with $f_{fundamental} = 28Hz$ having the largest general correlation between regions. As expected, with increasing noise, the relative correlation begins to decrease for most $f_{fundamental}$ values. Interestingly, with $\beta = 1.5$, the functional connectivity for $f_{fundamental} = 8Hz, 12Hz$ appears generally higher than those of $f_{fundamental} = 16, 20$. In comparison to the structural connectivity data (see Figure 16), the mean correlations for most band-passing frequencies appear higher than those seen in the single frequency model, especially for $\beta = 0.5, 1.5$. Additionally, across all β and band-passing ranges, there is much less of a pattern in relation to a specific range having a generally larger correlation to the structural connectivity data; for $\beta = 0.5$, the functional connectivity evaluated for $f_{fundamental} = 4Hz$ has the highest mean correlation to the structural connectivity data. In contrast, for $\beta = 1.5$ and 3, the functional connectivity matrices at $f_{fundamental} = 8Hz$ and 12Hz respectively have a higher correlation to the structural connectivity data.

C. Wilson-Cowan Extension

In our investigation, we have broadened the scope of the Stuart Landau model by integrating it with the supercritical Hopf bifurcation concept within the framework of the Wilson Cowan model [11]. This approach allowed us to manipulate the carrier frequency of network nodes by modulating timescales, maintaining a constant ratio between excitatory and inhibitory components. The selection of bifurcation parameters p_e and p_i, critical for the transition phases of the model, was meticulously aligned with previous studies [11] to ensure consistency with established boundary conditions. This alignment facilitates a direct comparison with Stuart Landau's model while exploring new dimensions of neural dynamics.

Our results, derived from applying signal processing techniques analogous to those documented in Deco et al's [1] influential work, reveal significant insights into the frequency-specific behaviour of neural networks. Through detailed analysis of the envelope frequency and the metastability of excitatory and inhibitory signals, we have identified patterns of neural activity. Adjustments to band-pass filtering parameters, beta, and coupling weights further elucidated the complex interplay between network topology and signal dynamics. This comprehensive analysis underscores the versatility of our extended model in simulating a broader spectrum of neural behaviours, thereby offering a deeper understanding of the intricate mechanisms underlying brain activity. Our findings not only corroborate the robustness of established models but also highlight the potential for novel theoretical frameworks to contribute to the evolving narrative of computational neuroscience.

Simulations were conducted with a fine temporal resolution, using a timestep (dt) of 0.001 seconds over a span of 400 seconds. The simulation incorporated a single-frequency approach, aligning the timescales of excitatory and inhibitory components (τ_e and τ_i, respectively) according to a Hopf bifurcation framework with a scaling factor of 3.5. The analysis encompassed a range of frequency bands—specifically, 10-14 Hz, 14-18 Hz, and 18-22 Hz paired with noise parameter (β) values to be set at 0.05, 0.1, and 0.5.

Observations from the simulations indicate that the correlation strength in the Envelope Functional Connectivity (FC) derived from excitatory signals consistently surpassed that of the inhibitory FC, as evidenced by the more intense colours in the corresponding heatmap visualizations Figure 14. In contrast, the inhibitory signal patterns displayed greater variability and appeared to align more closely with the brain's structural connectivity across all examined β values, a trend that was maintained across the frequency spectrum (as detailed in Figure 14).

IV. DISCUSSION

Discrepancies in the assignment of Parameters Upon the computation and reproduction of multiple figures, assumptions had to be made for parameters not previously defined. The time step dt, used in the Euler-Maruyama integration method, was found to be optimal at 0.001 for larger periods of time. Additionally, the sample rate used when band-pass and low-pass filtering was defined to be inversely proportional to the time step to keep the parameters consistent. Because of the computational cost of simulating for larger periods of time, the maximum simulated time was reduced to 300 seconds for the calculation of the envelope functional connectivity matrices and 10 seconds for CCD matrices.

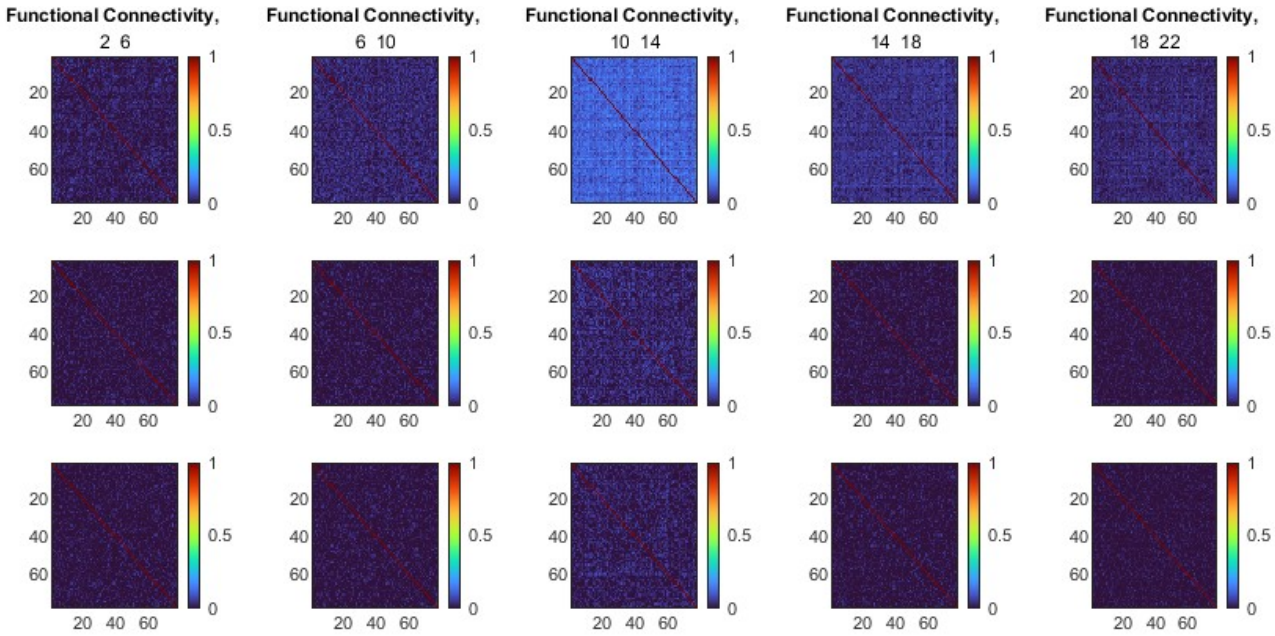

FIG. 10: **Envelope functional connectivity for single-frequency model.** Each row corresponds to a different noise strength, $\beta = 0.5, 1.5, 3$. The highest correlation between nodes is seen with nodes band-passed between $[10Hz, 14Hz]$ for all noise strengths, but gradually depletes with increased noise.

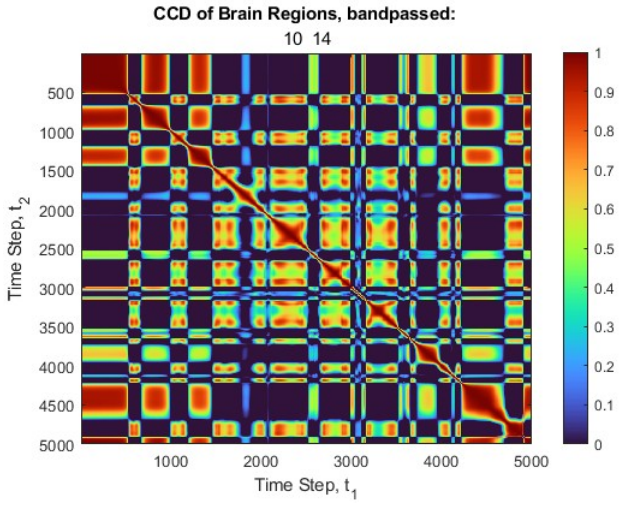

FIG. 11: **Coherence Connectivity Dynamics (CCD).** For ease of computation, parameters were updated as follows: $f_{fundamental} = 12Hz$, $dt = 0.002$, $sample\_rate = 2000$, $\beta = 0.5$. An observable "checkerboard" pattern indicates fluctuations in global synchrony over time.

Discrepancies in signal processing for the python and MATLAB While replicating the methodologies outlined in Deco [1], we employed Matlab and Python to construct a comprehensive brain model. We encountered distinct challenges while implementing band-pass and low-pass filters using the Butterworth filter from the Scipy package [14] in Python, as compared to Matlab. Specifically, Python's implementation required meticulous adjustment of parameters such as the filter order and the Nyquist frequency, which directly influence the filter's performance regarding frequency selectivity and roll-off characteristics. These parameters are pivotal in achieving the desired signal processing outcome, making their correct estimation crucial. The necessity for precise parameter tuning in Python's Scipy library starkly contrasts Matlab's more intuitive signal processing functions, which tended to abstract some of the complexities of filter design.
This highlights the inherent differences in signal processing capabilities between Matlab and Python, underscoring the significance of tool selection in computational research. While Matlab offers a more user-friendly environment for signal processing tasks, Python requires a deeper understanding of the theoretical underpinnings to manipulate signal characteristics effectively. Despite these challenges, the process of adapting signal processing techniques across different software platforms has provided valuable insights into the flexibility and precision required for computational modelling in neuroscience research.

Noise One of the fundamentally effective factors that we spotted in the model, which Deco [1] do not discuss sufficiently in their paper, is the noise parameter β. This is inherent in creating artificial neural networks, as the brain has various noise levels throughout. This noise can arise from intrinsic sources within individual neurons. An example of such a source is simply a spon-

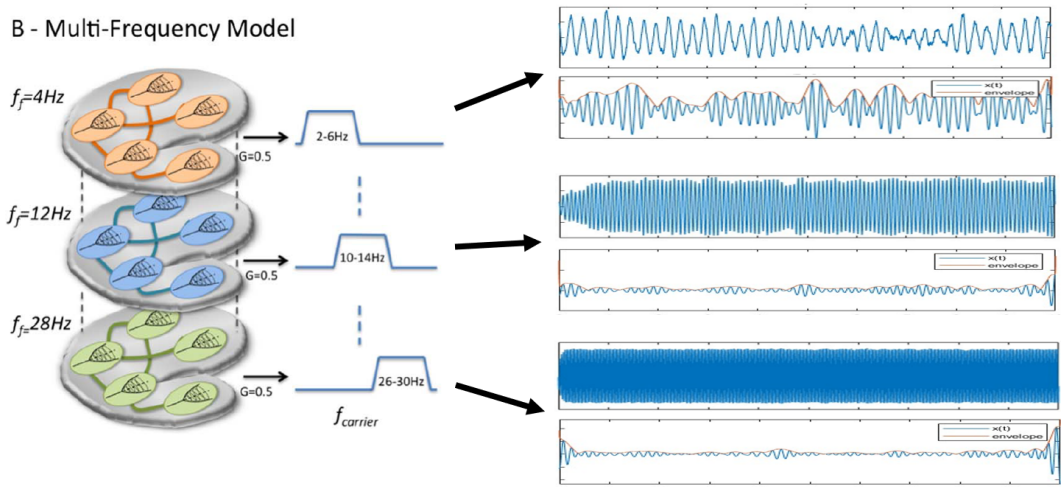

FIG. 12: **Visualisation of multiple-frequency model.** First, the fundamental frequency, $f_{fundamental} = 4 : 4 : 28$, is defined the same for all nodes, then the optimal band-pass range is set as $[f_{fundamental} - 2, f_{fundamental} + 2]$. Modification of figure in [1].

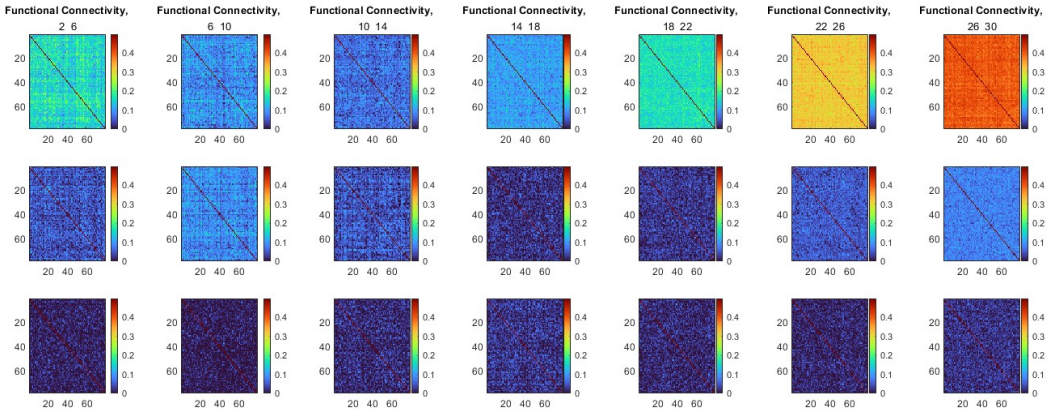

FIG. 13: **Envelope functional connectivity for multiple-frequency model.** Each row represents an increased noise strength, $\beta = 0.5, 1.5, 3$ Evidently, the general correlation increases as $f_{fundamental} = 4 : 4 : 28$ increases, especially with $\beta = 0.5$. Increasing the noise sufficiently removes said trends.

taneous neural activity arising from the stochastic firing of individual neurons, which consequently produces "background noise" in neural recordings and sometimes enhances synaptic efficacy and the responsiveness of cortical cells [15]. Other research has identified that "channel noise" is triggered by the probabilistic gating of voltage-dependent ion channels and actually limits the reliability of neuronal responses to identical stimuli – thus indicating how sparse brain activity may be, purely due to noise. The effects of the noise parameter β can be observed in Figures 15 and 16 wherein structural and functional connectivity were correlated after a range of bandpassing, and a mean correlation of the final matrix was taken, to be plotted against the frequency range. The optimal bandpass that Deco [1] state is 10-14Hz, was only prevalent when beta = 3 for the multiple-frequency model (see Figure 16). Although a consistent pattern of an optimal 10-14Hz can be seen in the single-frequency model (see Figure 10), we also observe drastic drops in mean correlation as beta increases. Future research should aim to study the optimal noise parameters for a given computational model and compare this against empirical data for verification.

Single-Frequency and Multiple-Frequency Models Both single-frequency and multiple-frequency models have been simulated with the expectation of recreating convincing correlations to structural connectivity data. The single-frequency model sets a fixed initial frequency of 12Hz for each brain region, then band-passes the signals at different frequency ranges, with the evaluation that a narrowband of $[10Hz, 14Hz]$ correlates best both to the findings of Deco as well as correlating best with the structural connectivity data. Conversely, with the multiple-frequency model,

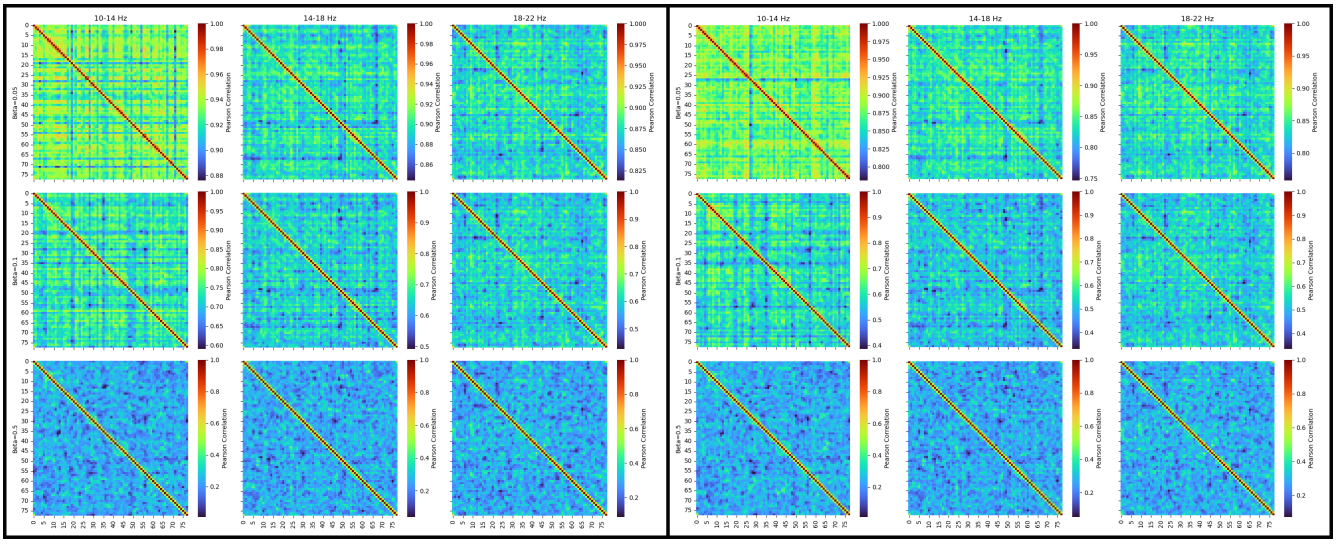

FIG. 14: **Comparative analysis of envelope functional connectivity in Wilson-Cowan model [11].** Two envelope FCs derived from the Wilson-Cowan hopf model under single frequency conditions, showcasing excitatory (left panel) and inhibitory (right panel) neural signals across three non-overlapping frequency bands, i.e., 10-14 Hz, 14-18 Hz and 18-22 Hz. The frequency dynamics are modulated by adjusting the timescale parameters $\tau_e = 0.03/\mathrm{n}$ and $\tau_i = 0.08/\mathrm{n}$, with $\mathrm{n} = 3.5$. The analysis considers three different beta values for noise, namely 0.05, 0.1 and 0.5, each associated with a separate row to explore the model's behaviour under different noise levels.

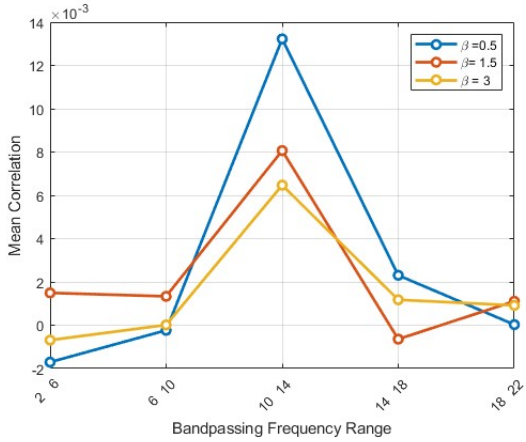

FIG. 15: **Scatter plot of mean correlation between the structural connectivity and functional connectivity of the single-frequency model.** The mean value of Pearson's correlation between the structural connectivity of the MEG data and the functional connectivity of the single-frequency model for each band-pass narrowband range is calculated. $[10Hz, 14Hz]$ evidently correlates more to the MEG data than other band-pass narrow bands for all $\beta = 0.5, 1.5, 3$, but the correlation decreases as β is increased.

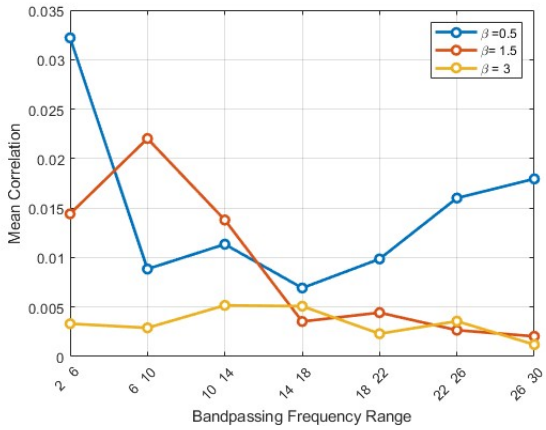

FIG. 16: **Scatter plot of mean correlation between the multiple-frequency model's structural connectivity and functional connectivity.** The same process as seen in 15 is used but adapted to the multiple-frequency model. A less coherent correlation is visible, with the optimal band-pass narrow band changing for every β value. However, the general correlation between structural connectivity and functional connectivities is higher than those seen in the single-frequency model.

all brain regions were initially fed the same fundamental frequency, and the signal was band-passed with a frequency range specific to the fundamental frequency; $[(f_{fundamental} - 2)Hz, (f_{fundamental} + 2)Hz]$ for $f_{fundamental} = 4 : 4 : 28$. Differing from the single-frequency model, using the envelope functional connectivity, general correlation seemed to generally increase with increasing fundamental frequencies, especially with $\beta = 0.5$; however, with varying β, the

optimal fundamental frequency changed in relation to correlating best to the structural connectivity. According to figures 15 and 16, the functional connectivity matrices of the multi-frequency model correlate better with the structural connectivity than the single-frequency model. Regions of the brain can generate signals of multiple frequencies, and so the conclusion that a model that incorporates the region generating multiple frequencies correlating to structural connectivity data makes sense.

Model Comparison The exploration of metastability in brain network simulations reveals a noteworthy distinction in the behaviour of the Stuart-Landau and Wilson-Cowan models [11] (see Figure 17), particularly when considering the parameter β as representative of noise within the system. In its portrayal of inhibitory signal dynamics, the Wilson-Cowan model displays a pattern (see Figure 14) that appears to align with the known structural connectivity of the brain more closely (see Figure 8). This alignment suggests an intriguing consistency that the simpler Stuart-Landau model struggles to match, especially under the influence of varying noise levels.

The envelope functional connectivity (FC) derived from the Wilson-Cowan model presents a compelling and reliable pattern, hinting at a greater degree of biological fidelity. This starkly contrasts with the Stuart-Landau model, which requires cautious interpretation when subjected to noise variations due to its propensity for oversimplification that may overlook the subtleties of brain dynamics. On the other hand, the Wilson-Cowan model demonstrates robustness against such noise perturbations, solidifying its standing as a more suitable candidate for modelling complex brain activities.

Furthermore, the Wilson-Cowan model's potential may be amplified when applied within a multi-frequency framework, offering a fertile ground for advanced analyses, such as characterizing the temporal evolution of synchronicity via cross-correlation dynamics (CCD). Such approaches could unveil the intricate temporal patterns of synchronization that are vital for understanding cognitive processes. Hence, the Wilson-Cowan model may emerge not only as a more robust alternative to its Stuart-Landau counterpart but also as a promising substrate for future investigations into the oscillatory nature of brain connectivity.

Our study does have several limitations that require consideration. Firstly, our findings are contingent upon various assumptions made during the model creation, including the selection of parameter values such as dt, noise, beta, simulation duration, and sample rate. These assumptions may introduce biases or inaccuracies into our results but were undeniably required given that the original paper did not explicitly outline parameters used for the majority of their simulations [1]. Additionally, our study lacks a comprehensive comparison of our model against a broader range of empirical evidence beyond the scope of the referenced paper, thus reducing the generalisability of our findings. Furthermore, while

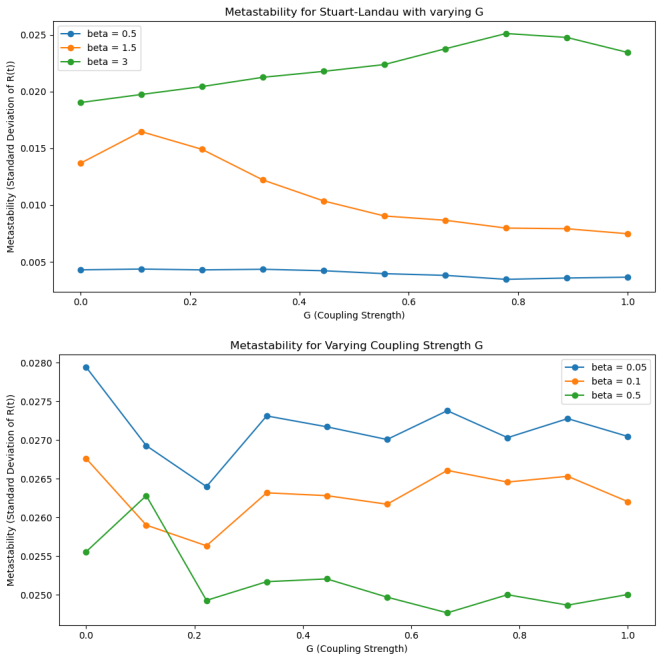

FIG. 17: **Discrepancies in Metastability Across Brain Network Models.** For the Wilson-Cowan model (bottom), metastability is relatively higher and stable across different β values. It significantly drops for lower $\beta = 0.5$ in the Stuart-Landau model (top).

our computational model demonstrates similarities to observed oscillatory neuronal behaviour and allows for predictions to be made, it simplifies the inherently intricate complexity of the brain. This further perpetuates the debate of whether computational models can indeed encapsulate such intricacy.

V. CONCLUSION

In summary, our findings provide several key insights into resting-state brain dynamics and functional connectivity by building on the work conducted by Deco [1]. Whilst we successfully replicated their conclusion that tends towards a multiple-frequency model of brain dynamics, we uncovered crucial oversights and possible errors in their original work. Model behaviour was not identical to that of Deco [1] and in some cases, envelope functional connectivity showed an astounding correlation compared to theirs. The possibilities of this difference remain endless, given that their original paper failed to report many parameter values and coherent model creation steps, as well as lacking in the provision of supplementary code. The assumptions made for this computational model come with an inherent lack of validity, which has demonstrated the little replicability and validity that their original model holds. Learning from this, this report clearly outlined all procedures taken to obtain the aforementioned results, as well as

venturing beyond the paper and running model simulations for varying parameters, paying particular attention to beta. It is evident that noise plays a much larger factor than their research assumed, and future research should aim to test how noise affects the reliability of biomedical modelling. This research also uncovered noticeable differences between Deco et al's (2017) model and the Wilson-Cowan model [11], the latter of which proved much more representative of empirically evidenced structural connectivity. Nevertheless, it is essential to acknowledge that our findings were limited by the assumptions made and the lack of generalizability of our findings. Moving forward, we suggest future research efforts focus on refining and expanding existing computational models, enhancing the accessibility and replicability of scientific papers and models, and conducting more neurophysiological studies to validate theoretical scenarios proposed in computational models. These endeavours will be crucial in confirming the accuracy of underlying assumptions and mechanisms, ultimately enhancing the validity, replicability, and reliability of computational models in neuroscientific research.

VI. ACKNOWLEDGEMENTS

All authors contributed equally to this work. They engaged in research, planning, code production, figure creation, analysis and writing of the report.

We would like to express gratitude to Stephen Coombes, for his kind and consistent academic guidance in understanding and re-creating computational models.

REFERENCES

1. Deco G, Cabral J, Woolrich MW, Stevner ABA, Hartevelt TJ van, and Kringelbach ML. Single or multiple frequency generators in on-going brain activity: A mechanistic whole-brain model of empirical MEG data. NeuroImage. 2017 May 15; 152:538–50
2. Xu Y, Liu X, Cao X, Huang C, Liu E, Qian S, Liu X, Wu Y, Dong F, Qiu CW, Qiu J, Hua K, Su W, Wu J, Xu H, Han Y, Fu C, Yin Z, Liu M, Roepman R, Dietmann S, Virta M, Kengara F, Zhang Z, Zhang L, Zhao T, Dai J, Yang J, Lan L, Luo M, Liu Z, An T, Zhang B, He X, Cong S, Liu X, Zhang W, Lewis JP, Tiedje JM, Wang Q, An Z, Wang F, Zhang L, Huang T, Lu C, Cai Z, Wang F, and Zhang J. Artificial intelligence: A powerful paradigm for scientific research. The Innovation. 2021 Nov 28; 2:100179
3. Abbott LF and Vreeswijk C van. Asynchronous states in networks of pulse-coupled oscillators. Physical Review E. 1993 Aug 1; 48. Publisher: American Physical Society:1483–90
4. Brunel N and Wang XJ. What determines the frequency of fast network oscillations with irregular neural discharges? I. Synaptic dynamics and excitation-inhibition balance. Journal of Neurophysiology. 2003 Jul; 90:415–30
5. Honey CJ, Kötter R, Breakspear M, and Sporns O. Network structure of cerebral cortex shapes functional connectivity on multiple time scales. Proceedings of the National Academy of Sciences of the United States of America. 2007 Jun 12; 104:10240–5
6. Cabral J, Hugues E, Sporns O, and Deco G. Role of local network oscillations in resting-state functional connectivity. NeuroImage. 2011 Jul 1; 57:130–9
7. Cabral J, Kringelbach ML, and Deco G. Exploring the network dynamics underlying brain activity during rest. Progress in Neurobiology. 2014 Mar; 114:102–31
8. Brookes MJ, Hale JR, Zumer JM, Stevenson CM, Francis ST, Barnes GR, Owen JP, Morris PG, and Nagarajan SS. Measuring functional connectivity using MEG: Methodology and comparison with fcMRI. NeuroImage. 2011 Jun 1; 56:1082–104
9. Hillebrand A, Tewarie P, Dellen E van, Yu M, Carbo EWS, Douw L, Gouw AA, Straaten ECW van, and Stam CJ. Direction of information flow in large-scale resting-state networks is frequency-dependent. Proceedings of the National Academy of Sciences of the United States of America. 2016 Apr 5; 113:3867–72
10. Qian L, Zhang Y, Zheng L, Shang Y, Gao JH, and Liu Y. Frequency Dependent Topological Patterns of Resting-State Brain Networks. PLOS ONE. 2015 Apr 30; 10. Publisher: Public Library of Science:e0124681
11. Coombes S, Beim Graben P, Potthast R, and Wright J, eds. Neural Fields: Theory and Applications. Berlin, Heidelberg: Springer, 2014
12. Higham. DJ. An Algorithmic Introduction to Numerical Simulation of Stochastic Differential Equations. SIAM Review. 2001 Jan; 43. Publisher: Society for Industrial and Applied Mathematics:525–46
13. AAL atlas. Nilearn. Available from: https://nilearn.github.io/modules/description/aal_SPM12.html
14. SciPy. Available from: https://scipy.org/
15. Destexhe A, Rudolph M, and Paré D. The high-conductance state of neocortical neurons in vivo. Nature Reviews Neuroscience. 2003 Sep; 4. Publisher: Nature Publishing Group:739–51